





# 3D-printed wideband reflectarray antennas with mechanical beam-steering

cambridge.org/mrf

Andrea Massaccesi<sup>1</sup> , Michele Beccaria<sup>1</sup> , Valentina Bertana<sup>2,3</sup>,  
Simone Luigi Marasso<sup>2,3,4</sup>, Matteo Cocuzza<sup>2,3,4</sup>, Gianluca Dassano<sup>1</sup> and  
Paola Pirinoli<sup>1,5</sup>

## Research Paper

**Cite this article:** Massaccesi A, Beccaria M, Bertana V, Marasso SL, Cocuzza M, Dassano G, Pirinoli P (2024) 3D-printed wideband reflectarray antennas with mechanical beam-steering. *International Journal of Microwave and Wireless Technologies* **16**(1), 21–29. <https://doi.org/10.1017/S1759078723000776>

Received: 31 January 2023  
Revised: 27 May 2023  
Accepted: 30 May 2023

### Keywords:

3D-printing; additive manufacturing; perforated dielectric; periodic structures; reflectarray antennas

**Corresponding author:** Andrea Massaccesi;  
Email: [andrea.massaccesi@polito.it](mailto:andrea.massaccesi@polito.it)

<sup>1</sup>Department of Electronics and Telecommunications, Politecnico di Torino, Torino, Italy; <sup>2</sup>Department of Applied Sciences and Technology, Politecnico di Torino, Torino, Italy; <sup>3</sup>Chilab-Materials and Microsystems Laboratory, Politecnico di Torino, Chivasso (TO), Italy; <sup>4</sup>IMEM-CNR, Parma, Italy and <sup>5</sup>IEIT-CNR, Torino, Italy

### Abstract

This paper investigates the performance of 3D-printed dielectric reflectarray antennas (RAs) with wideband behavior and beam-steering capabilities. The designed unit cell consists of a single-layer dielectric element perforated with a square hole, whose side is used to control the local variation of the reflection coefficient. The numerical analysis of the unit cell and of first  $52 \times 52$  reflectarray working in Ka-band, whose scanning capabilities are tested just moving the feed along an arc, confirms that the unit cell has a stable behavior with respect to both the frequency and the direction of arrival of the incident field. In view of these promising capabilities, the proposed unit cell is used to design a bifocal reflectarray with the same size and working in the same frequency band of the first one. Its numerical characterization and the measurements of a prototype prove that the RA is able to provide less than 0.8 dB of gain losses over a scanning range of  $\pm 40^\circ$  in the vertical plane, while the bandwidth varies between 13.5% and 28%, depending on the pointing direction. The obtained results demonstrate the effectiveness of the proposed approach and highlight the potential of 3D-printing technology for producing high performance, cost-effective RAs with wideband behavior and excellent beam-steering features.

## Introduction

Next-generation antennas will need to be characterized by a wideband behavior and by reconfigurability to generate multiple or scanning beams. To achieve these aims, several options have been proposed, and among them, the possibility to use reflectarray antennas (RAs) [1, 2] has also been considered. Despite their copious advantages, RAs also present some drawbacks, the principal of which is a reduced bandwidth, essentially due to the intrinsic narrow bandwidth of single-layer printed elements, widely used for the realization of the RA unit cells (UCs) and to the frequency dependence of the path from the feed to the different points on the planar surface. To overcome this limitation, the use of elements with more degrees of freedom, printed on different layers, as in [3, 4] or on the same dielectric substrate [5–9], were introduced. Recently, the design of dielectric-only RAs is becoming popular, especially at mm-waves and sub-THz frequencies, where the metal losses are significant. Among the other potentialities, dielectric-only structures present a wider bandwidth and a low manufacturing cost that makes feasible the manufacturing of radiating elements with arbitrary shapes. On the other hand, they are also responsible for some restrictions, related to the available materials, in most of the cases characterized by a low value of the relative dielectric constant and by high losses, to the printer resolution, that affects the minimum realizable size, and to the size of the printing plate.

Several examples of 3D-printed dielectric-only reflectarrays are available in literature. The configurations proposed in [10, 11] use dielectric parallelepiped resonators as UCs, whose height is varied to control the phase of the reradiated field. The 3D-printed prototype in [10] has an aperture of  $12\lambda \times 12\lambda$  and shows a 1-dB bandwidth of almost 10%, while that in [11] is characterized by a size of  $20.5\lambda \times 20.5\lambda$  at sub-THz frequencies and 1-dB bandwidth slightly lower than 21%. The configuration in [12] uses hemi-ellipsoidal dielectric resonators as reradiating elements: the designed antenna has an aperture size of  $5.5\lambda \times 5.5\lambda$  and 1-dB bandwidth of 11.2%. In [13], a C-shaped dielectric UC with height approximately equal to  $1.5\lambda$  is adopted for the design of a center-fed RA with diameter of  $10\lambda$ . The 1-dB bandwidth in the case in which the radiated field is linearly polarized is slightly smaller than 12%. The reflectarray in [14] has an aperture of  $11.2\lambda \times 11.2\lambda$ , discretized with cross-shape elements and provides a 1-dB bandwidth of 10.7%, while in [15], a Kirigami inspired two-stage snapping-like element is introduced for the realization of a  $11.37\lambda \times 11.37\lambda$  RA with a 1-dB bandwidth of 16.3%. Finally, the solution in [16] adopts two orthogonal dielectric cuboids to design a  $10.7\lambda \times 10.7\lambda$  aperture that is able to generate a dual circularly polarized field over a 1-dB bandwidth  $\approx 13\%$ .

For what concerns the multi or scanning beam capability, the most straightforward solution is to design a reflectarray in which the behavior of the UC is controlled through active elements such as pin diodes [17–22], varactors, [23–26], and MEMS switches [27] or using liquid crystal [28–30] or liquid metal [31] for its realization. All these choices strongly affect the complexity and the cost of the antenna, and therefore possible alternatives have been studied. In few projects, as the one in [32], are aimed to reduced the control points in the active reflecting surface, in other configurations, the RA is passive and the beam-steering is obtained by mechanically rolling the aperture [33] or more commonly moving mechanically the feed or using a feed array to change the direction of arrival of the field impinging on the reflecting surface [34–36].

Despite its greater simplicity, such an antenna has some degradations of its radiation performance, as the enlargement of the main beam; an increase in the side-lobe level (SLL); a lowering of the maximum gain, which further decreases over the scan range; and a narrowing of the bandwidth. To improve the RA features, different techniques have been proposed, as that of designing a bifocal [37, 38] or a multi-focal [39] reflectarray; in [40], the RA is designed to behave as a quasi-spherical reflector, while in [41], the planar reflector is rotated in addition to the feed to cover a larger scan range. Finally, the results summarized in [37, 42] prove that a pseudo-stochastic optimization algorithm can be fruitfully adopted to design a beam-scanning reflectarray with enhanced performance.

As for the bandwidth, the reflectarray beam-scanning capabilities also depend on the properties of the UC. In fact, its behavior is affected by the direction of arrival of the incident field, and hence when it changes, the UC generally does not provide the required phase compensation, and this results in a degradation of the antenna radiation properties. To reduce this effect, it is therefore useful to adopt a proper UC in addition to a suitable design procedure.

In this context, the possibility of using a UC alike the one introduced in [43] for the realization of a beam-steering RA is investigated. Some preliminary numerical results on the scanning beam behavior of an RA consisting of  $52 \times 52$  are already collected in [44], but the UC adopted there, as the one in [43], does not fulfil the constraints imposed by the Additive Manufacturing (AM) technique selected for the antenna realization even if the results in [43, 44] confirm that the UC possess proper features for its use in the design of a scanning beam reflectarray with enhanced bandwidth. Here, the limitations introduced by the AM are taken into account and a printable version of the UC is defined, as is described in the section “Dielectric unit cell.” To verify its features and in particular its dependence from the angle of incidence, first, a single-focus RA is designed, and then its beam-steering capability is checked rotating the feed along an arc. In view of the encouraging numerical results summarized in subsection “Single focus RA: design and numerical analysis,” a bifocal RA is finally designed and manufactured. The numerical analysis and the experimental characterization of the prototype reported in the subsection “Bifocal RA: design, manufacturing, numerical and experimental characterization” show that the gain scan losses are lower than 0.8 dB over a scanning range of  $\pm 40^\circ$ , while the bandwidth varies between 13.5% and 28% over this interval.

### Dielectric unit cell

The adopted UC is an optimized version of those introduced in [43, 44]. As shown in the inset of Fig. 1, it consists in a dielectric

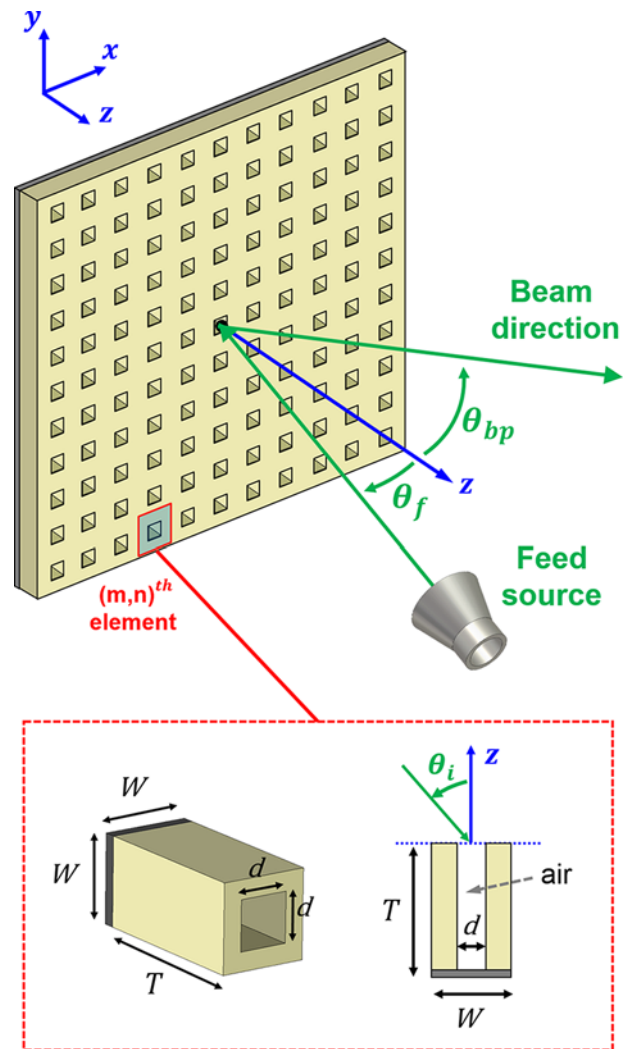
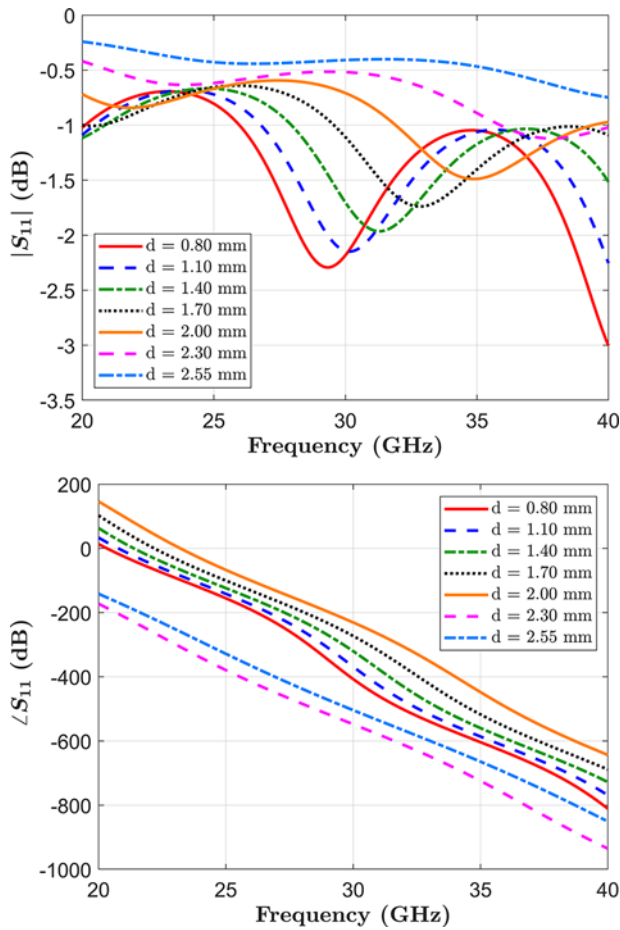


Figure 1. Sketch of the antenna configuration, with the UC in the inset.

parallelepiped with square basis, backed on a metallic ground plane, and having a square hole in the center, whose side  $d$  is varied to control the reflection coefficient  $S_{11}$ , while its height  $T$  is kept constant. The change of the hole size corresponds to modify the ratio between the quantity of dielectric material and air in the UC, resulting in a variation of its effective dielectric constant.

To make possible the printing of the UC with an AM technique, and in particular with a PolyJet printer, a suitable dielectric material must be used. Here, the chosen material is the 3D-printable resin *VeroWhitePlus™* provided by Stratasys<sup>®</sup> and characterized by  $\epsilon_r = 2.77$  and  $\tan \delta = 0.021$ , which is the same used in [45, 46]. The UC has been designed in Ka-band at the operating frequency  $f_0 = 30$  GHz. Since the structures proposed in [43, 44] were not suitable for 3D printing, a new version of the UC was optimized to maximize its performance while taking into account the limitations of the AM process. To determine the appropriate geometrical parameters for the UC that would allow for its fabrication, several test samples of dielectric sheets with square holes of varying sizes and heights were printed. After a thorough analysis, it was found that for small holes, the actual value of  $d$  was significantly smaller, and there was an increased risk of unwanted polymerization of small resin residues that could clog up the hole. In order to solve



**Figure 2.** Unit cell: Variation of the simulated reflection coefficient  $S_{11}$  with the frequency for different values of  $d$ . Top: amplitude. Bottom: phase. (UC dimensions:  $W = 3$  mm,  $T = 0.8$  mm,  $d = [0.8, 2.55]$  mm).

these issues, it was determined that the height of the UC should be maintained at a minimum of 6 mm and the size of the holes  $d$  should be varied within the range (0.8, 2.55) mm. This strategy aims to prevent systematic printing errors and to ensure that the holes are as accurate as possible. The optimal geometric parameters for the UC that satisfy the aforementioned requirements and maximize the performance are the following:  $W = 0.3\lambda_0 = 3$  mm,  $\lambda_0$  being the wavelength evaluated at  $f_0$ ,  $T = 0.8\lambda_0 = 8$  mm, while  $d$  can vary between 0.8 mm and 2.55 mm. They are obtained following an optimization process organized in the three steps listed below.

- (1) Choice of the size  $W$  of the UC: a smaller value guarantees a better sampling of the aperture and improves the antenna bandwidth but reduces the possible range of variation for the hole size  $d$ .
- (2) Determination of the range of variation of the hole size  $d$ : if it is larger, the range of variation for the phase of the reflection coefficient is wider, but either too small or too large values for  $d$  must be avoided since they correspond to a UC that cannot be manufactured.
- (3) Selection of  $T$ : increasing the height of the UC, it is possible to enlarge the range of variation for the phase of  $S_{11}$ , but at the cost of worsening of the losses introduced by the material and of a more bulky structure.

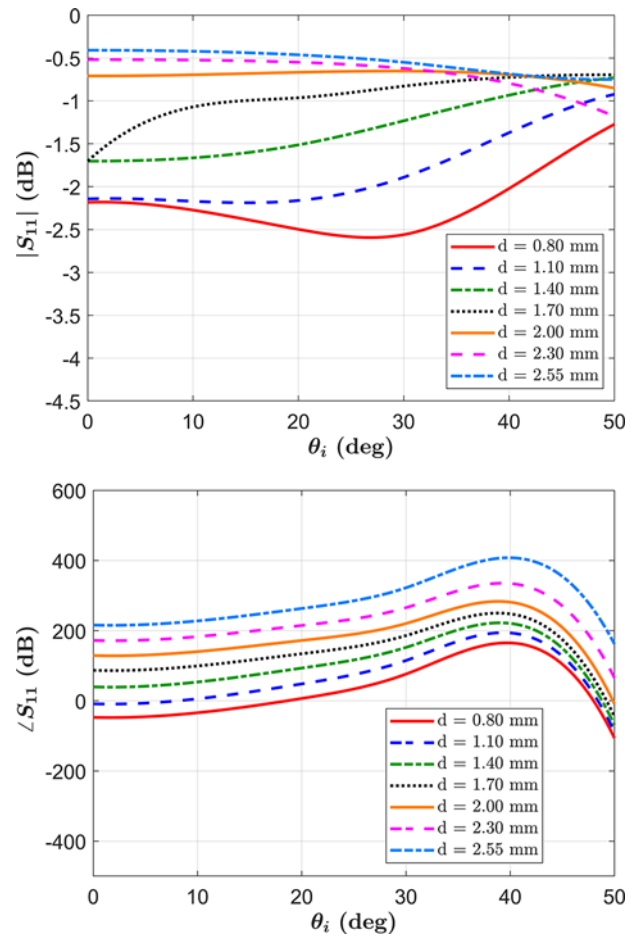


**Figure 3.** Unit cell: Variation of the simulated reflection coefficient  $S_{11}$  with the angle of incidence  $\theta_i$  at 30 GHz for different values of  $d$ . Top: amplitude. Bottom: phase (UC dimensions:  $W = 3$  mm,  $T = 0.8$  mm,  $d = [0.8, 2.55]$  mm).

In Fig. 2, the frequency behavior of the amplitude (top) and phase (bottom) of the reflection coefficient is plotted for different values of the hole size. It can be noticed that the phase varies linearly over the entire frequency range and that its behavior is almost the same for all the considered values of  $d$ , as proved by the fact that the different lines are almost parallel; the amplitude of  $S_{11}$  is never lower than  $-1.5$  dB when  $d \geq 2$  mm, while its value decreases for smaller holes due to the increase of losses. The dependence of the reflection coefficient from frequency, and in particular the linear behavior of the phase, confirms the wide band aptitude of the UC.

Since the UC would be used for the design of a beam-steering RA, its dependence from the direction of arrival of the incident field is also studied. In Fig. 3, the variation of the amplitude (top) and phase (bottom) of  $S_{11}$  is plotted with the angle of incidence  $\theta_i$ , evaluated for different values of  $d$  at the design frequency  $f_0$ . As can be seen from these results,  $\angle S_{11}$  does not change significantly till  $\theta_i = 40^\circ$ , while the amplitude of the reflection coefficient behaves in a different way depending on the hole size. In particular, when it is small,  $|S_{11}|$  reaches values even below  $-2.5$  dB for  $\theta_i \approx 30^\circ$ . For larger  $d$ , the influence of the direction of arrival of the incident field is negligible, and this confirms the possibility to use the considered UC for the design of a beam-steering reflectarray.

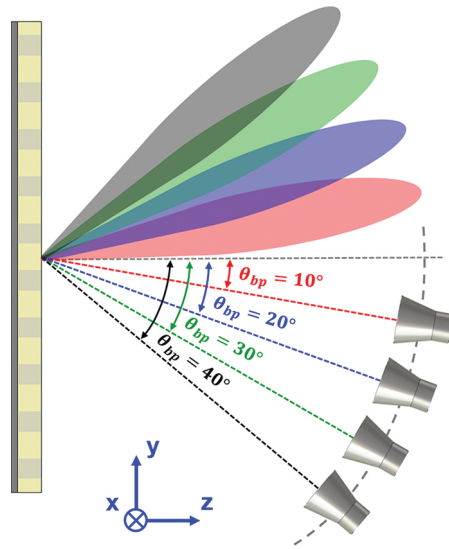


**Figure 4.** Beam-scanning reflectarray mechanism obtained moving the feed in the vertical plane along a circular arc with radius  $F$  for different scanning angles.

### Beam steering reflectarray

The UC previously discussed has been adopted for the design of two reflectarrays having the same configuration of the RA depicted in Fig. 1. Both the RAs have been designed with a side  $D = 15.6\lambda_0$ , corresponding to a discretization in 2704 reradiating elements. The aperture is illuminated by a 3D-printed smooth wall horn [47], whose radiation pattern can be modeled as  $\cos(\theta)^q$  with  $q = 12.5$ . The  $F$  distance between the phase center of the feed and the center of the planar aperture is 186 mm ( $F/D \sim 1.2$ ). This value of  $F$  was chosen to optimize the illumination taper and the aperture efficiency of the reflectarray. Using this distance, the resulting edges taper is equal to  $-9.5$  dB. The beam-scanning is obtained moving the feed in the vertical plane along a circular arc with radius  $F$ . A sketch of the antenna beam-scanning mechanism, with the information on the coordinate reference system, is shown in Fig. 4: referring to it, the vertical plane is the  $yz$ -plane, where the beam pointing direction  $\theta_{bp}$  changes consequently to the rotation of the feed.

### Single focus RA: design and numerical analysis

In order to check the scanning capabilities of the UC, first, a single focus reflectarray is designed to produce a pencil beam in the broadside direction when it is center-fed, which corresponds to the beam pointing angles ( $\theta_{bp} = 0^\circ$  and  $\varphi_{bp} = 0^\circ$ ). The required phase distribution that produces this beam feature is shown in Fig. 5 and can be calculated as follows:

$$\phi_R(x_m, y_n) = k_0(d_{mn} - (x_m \cos(\varphi_{bp}) + y_n \sin(\varphi_{bp})) \sin(\theta_{bp})), \quad (1)$$

where  $d_{mn}$  is the distance from the phase center of the feed to each cell, while  $(x_m, y_n)$  represent the position of each element in the RA aperture. The design was carried out using only the phase curves obtained in the case of normal incidence. This assumption can be considered reliable due to the favorable behavior of the UC under oblique incidence, seen in the previous sections. The resulting RA

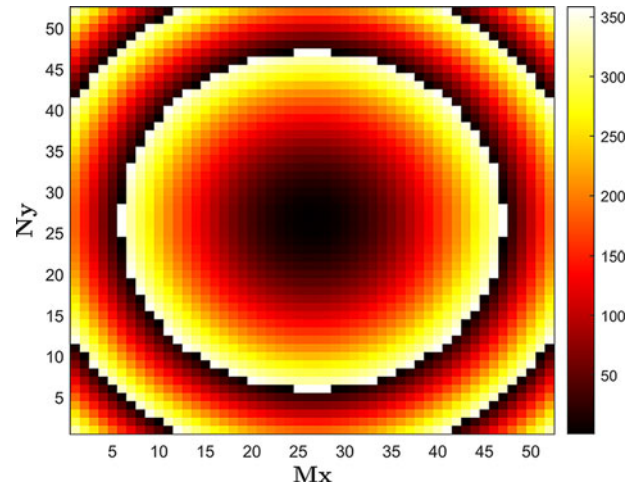


**Figure 5.** Required phase distribution of the  $52 \times 52$  single focus RA.  $M_x$  and  $N_y$  refer to the number of elements in  $x$  and  $y$  directions, respectively.

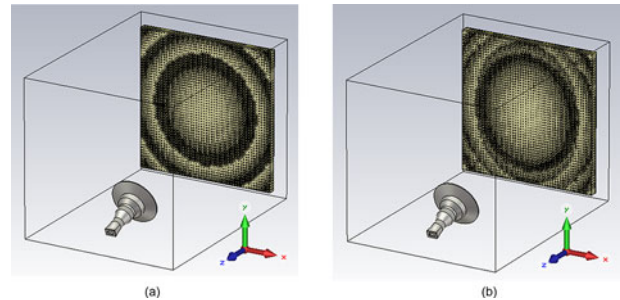


**Figure 6.** Three-dimensional (3D) CAD model of the two designed dielectric reflectarrays: (a) single focus and (b) bifocal.

is then numerically analyzed with CST Microwave Studio, not considering the position of the feed for which the reflecting surface is designed but moving the horn along the circular arc of radius  $F$  in such a way that  $\theta_{bp}$  varies between  $10^\circ$  and  $40^\circ$ . A picture of the 3D CAD model of the single focus RA is shown in Fig. 6(a). Because of the symmetry of the structure, this corresponds also to cover the range of variation going from  $-40^\circ$  to  $-10^\circ$ , so that a total scan range given by  $[-40^\circ, -10^\circ] \cup [10^\circ, 40^\circ]$  can be achieved. For sake of clearness, just the results related to the positive scanning range  $[10^\circ, 40^\circ]$  are plotted.

The obtained radiation patterns in the vertical ( $E$ -) plane and for different pointing directions are plotted in Fig. 7, while the solid line curve in Fig. 8 represents the variation of the gain with the pointing direction for this RA. As expected, the radiation patterns and in particular the main beam degrade over the considered scanning range; however, moving the pointing direction from  $\theta_{bp} = 10^\circ$  to  $\theta_{bp} = 30^\circ$ , the gain decreases by only 1.1 dB. A more important degradation of the radiation performance can be noticed for the pattern pointing to  $\theta_{bp} = 40^\circ$  characterized by a gain loss of almost 3.5 dB and an enlargement of the main beam.

In Fig. 9, the effect of the beam-steering on the bandwidth is shown; also in this case, the solid line curve refers to the single focus reflectarray, and it reveals that the 1-dB gain bandwidth is slightly lower than 19% for  $\theta_{bp} = 10^\circ$ , while as it can be predicted by the behavior of the gain, it increases up to 38% for  $\theta_{bp} = 40^\circ$ .

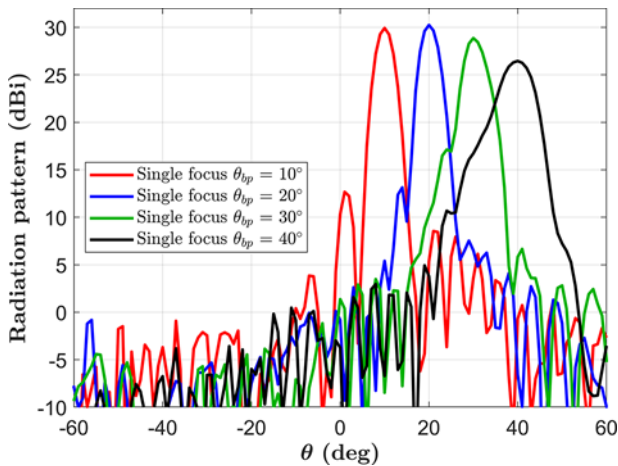


**Figure 7.** Simulated radiation patterns in the vertical plane for four different scanning angles, obtained through the numerical analysis of the single focus reflectarray.

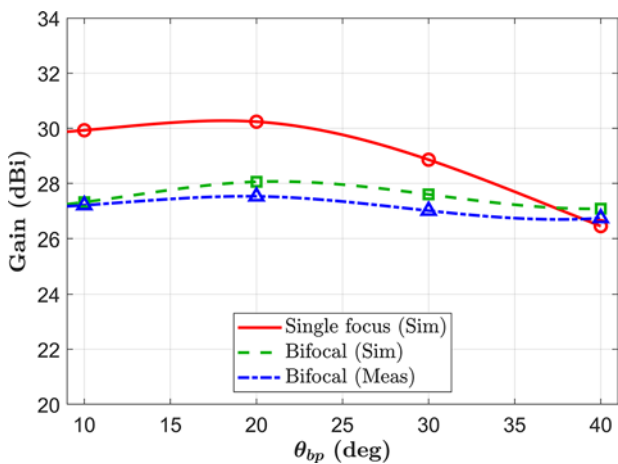


**Figure 8.** Variation of the gain with the pointing direction. Solid line: simulated single focus RA; dashed line: simulated bifocal RA; and dash-dotted line: measured bifocal RA.

The results on both the scanning performance and the bandwidth are promising, and suggest that the proposed UC is a potentially good candidate for designing reflectarrays with scanning beam capabilities and enhanced bandwidth with respect to other solutions.

**Bifocal RA: design, manufacturing, numerical, and experimental characterization**

Since the analysis summarized above confirms the suitability of the UC, it is adopted for the design of a bifocal reflectarray that is expected to have improved scanning features with respect to the single focus configuration. In order to cover the same scan range considered in the subsection “Single focus RA: design and numerical analysis” and taking into account the structure symmetries, the bifocal RA is designed to provide the phase distribution  $\Phi_{mean}$  shown in Fig. 10 and obtained as:

$$\Phi_{mean} = \frac{\Phi_1 + \Phi_2}{2}, \tag{2}$$

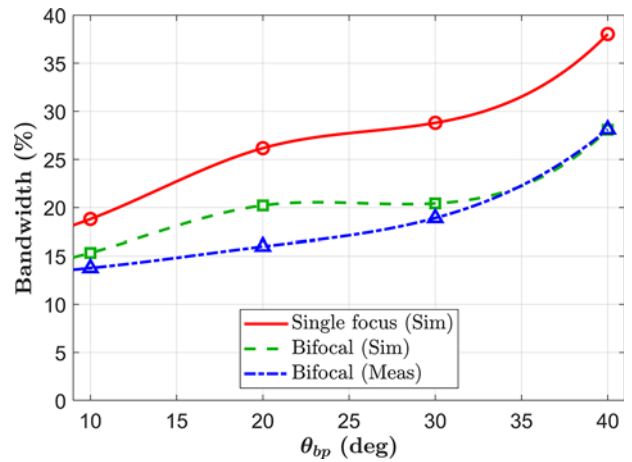


**Figure 9.** Variation of the 1-dB gain bandwidth with the pointing direction. Solid line: simulated single focus RA. Dashed line: simulated bifocal RA. Dash-dotted line: measured bifocal RA.

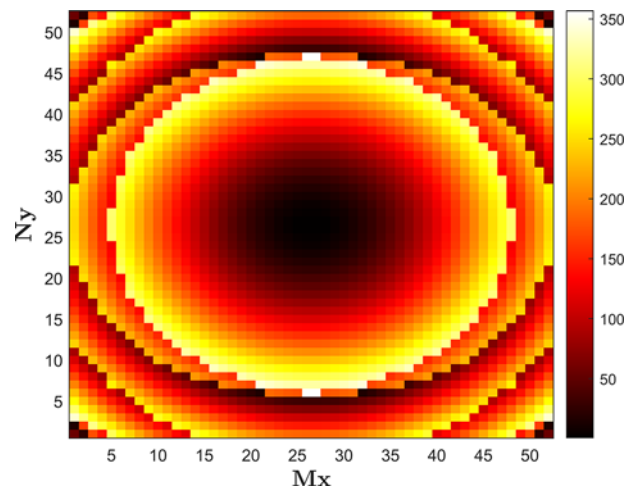
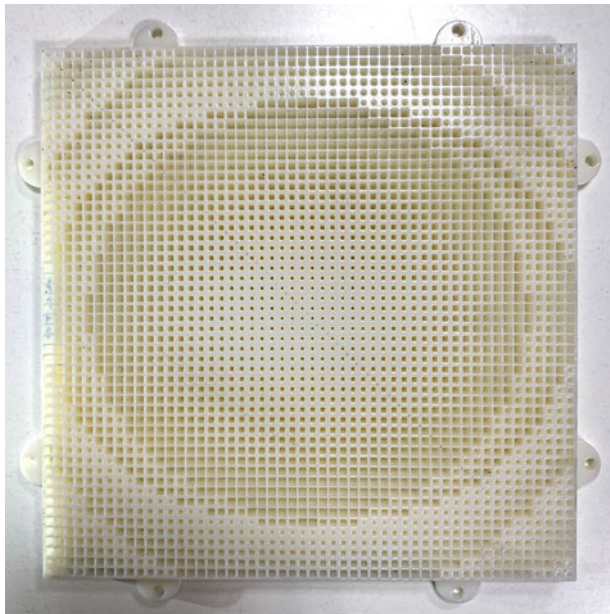


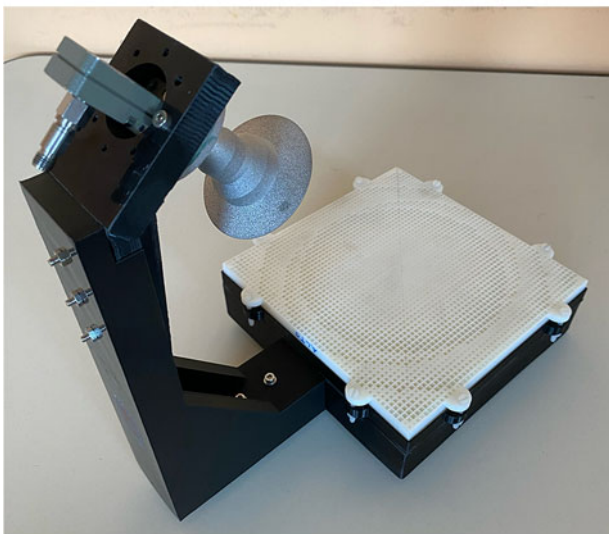
**Figure 10.** Required phase distribution of the 52x52 bifocal RA.  $M_x$  and  $N_y$  refer to the number of elements in  $x$  and  $y$  directions, respectively.

where  $\Phi_1$  and  $\Phi_2$  are the phase distributions required to generate a collimated beam pointing to  $\theta_{bp1} = -30^\circ$  and  $\theta_{bp2} = +30^\circ$ , respectively. These distributions were obtained using Eq. 1 and using the phase curve related to normal incidence for both focal points.

The designed bifocal reflectarray has been simulated with CST MS and a picture of its 3D CAD model is shown in Fig. 6(b). A prototype of the reflectarray was manufactured using the Polyjet-based machine Objet30 (provided by Stratasys®) and then experimentally characterized. From the picture in Fig. 11(a), it appears that due to the required phase distribution and to the chosen additional reference phase, in the central part of the reflectarray, the UCs are characterized by smaller values of the holes, which increase going to the edges. This configuration is designed also in view of the results on the dependence from the incidence angle of the UC summarized in Fig. 3 and already discussed. Since the limitations introduced by the adopted 3D printer are taken into account in the UC design, none of the smaller holes results to be blocked. The holes set all around the RA surface are added for fixing it to the metallic ground plane through the use of a frame manufactured with FDM 3D printing technique. Figure 11(b) shows the entire antenna structure.



(a)



(b)

**Figure 11.** 3D-printed dielectric bifocal reflectarray with mechanical beam-steering: (a) prototype top view and (b) complete antenna structure.

In Fig. 12, both the simulated and the measured radiation patterns for different pointing directions at the design frequency are plotted. First, it is worth to note the very good agreement between the numerical and experimental results, confirmed by the performance summarized in Table 1. As expected, the radiation patterns of the bifocal RA are better than those of the single focus configuration, since they are characterized by a more constant gain over the entire scan range and consequently by a less remarkable enlargement of the beam width. As emerges from Table 1, both the numerical analysis and the measurements of the bifocal RA confirm that the HPBW changes less than 1 degree over the entire scan range, the SLL is always below  $-13.8$  dB and the maximum gain scan loss is about  $0.8$  dB, as also shown by the dashed and dot-dashed line curves in Fig. 8, that are almost flat. As expected,

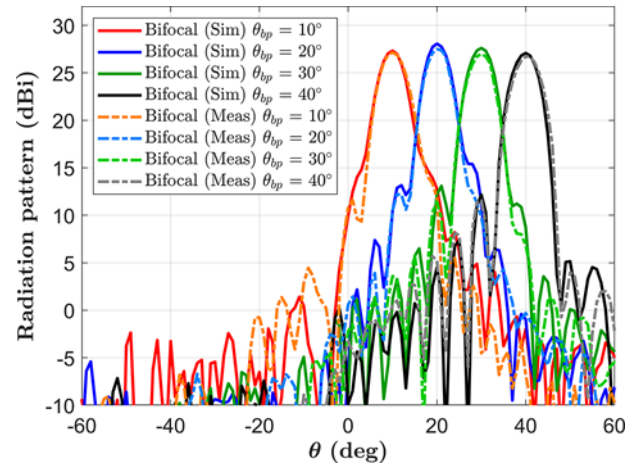


**Figure 12.** Radiation patterns in the vertical plane for four different pointing directions, obtained through the numerical analysis (solid line) and the measurement (dashed line) of the bifocal reflectarray.

the gain slightly reduces for pointing direction closer to broad-side, which are farther from those considered for the design of the bifocal surface. Moreover, as typical of a bifocal configuration, the maximum gain is lower of almost  $2$  dB than the one of the single focus configuration, but this is the price to pay for keeping it more constant over the scan range. As expected, the gain reduction entails also a lowering of the aperture efficiency, that for the single focus configuration, when the pointing direction is that for which the antenna is designed, is of the order of  $40\%$ .

For what concerns the  $1$ -dB gain bandwidth, from Fig. 9, it appears that it is reduced with respect to that of the single focus configuration. Nevertheless, the results reported in the third row of Table 1 prove that it is slightly lower than  $14\%$  for  $\theta_{bp} = 10^\circ$ , but it increases in the other considered pointing directions. This is a remarkable achievement for a relatively large aperture, since larger structures are generally more challenging to design and analyze, requiring higher levels of accuracy and uniformity. This adds even more significance to the presented results compared to smaller structures typically reported in the literature.

Finally, in Table 2, the measured performance of the bifocal reflectarray is compared with those of other passive scanning beam RAs. Comparing the data relating to their size (row 3), it appears that the antenna proposed here has the largest aperture: this is to take into account discussing its radiating features, since it is well known that properties as the bandwidth decrease with the increasing of the aperture. For what concerns the scan range, only that covered by the RA in [35] is larger than the one considered here. The most remarkable performance of the designed reflectarray is the gain loss  $\Delta G$ , equal to  $0.8$  dB over the entire scan range, significantly lower than the value obtained in [35] and comparable with the value reported in [37], which, however, refers to a smaller configuration and a narrower scan range. It is worth to notice that if the extremes of the variation interval for the pointing angle are reduced to  $\pm 30^\circ$ , as considered in [37, 38], the measured gain scan loss provided by the reflectarray presented here is of the order of  $0.2$  dB only. The comparison among the maximum achieved  $1$ -dB gain bandwidth confirms the good properties of the dielectric UC: as a matter of fact, the proposed RA and that in [38] have a band that is significantly wider than the other two reported structures.

**Table 1.** Summary of the simulated and measured bifocal RA performance for different pointing directions

Method	Bifocal (Sim)	Bifocal (Meas)	Bifocal (Sim)	Bifocal (Meas)	Bifocal (Sim)	Bifocal (Meas)	Bifocal (Sim)	Bifocal (Meas)
$\theta_{bp}$ (deg)	$\pm 10$	$\pm 10$	$\pm 20$	$\pm 20$	$\pm 30$	$\pm 30$	$\pm 40$	$\pm 40$
Gain (dBi)	27.3	27.2	28.1	27.5	27.6	27.0	27.1	26.7
$\eta_{ap}$	17.6	17.2	20.9	18.5	18.8	16.4	16.7	15.4
1-dB BW (%)	15.3	13.8	20.2	16.0	20.4	18.9	28.1	28.1
HPBW 9deg)	6.1	6.5	5.8	5.9	6.2	6.1	6.5	6.9
SLL (dB)	-13.4	-13.8	-12.7	-15.1	-14.5	-15.6	-14.9	-15.3

**Table 2.** Comparison between the measured features of the proposed passive bifocal beam-scanning RA and those of other similar configurations available in the literature

Reference	[37]	[35]	[38]	This work
Frequency [GHz]	32	12	30	30
Aperture ( $\lambda_0^2$ )	227	64	129.3	243.36
F/D	0.725	1	2	1.2
Design	Bifocal	PMM	Bifocal	Bifocal
Dielectric	N	N	Y	Y
Scan range	$\pm 30^\circ$	$\pm 45^\circ$	$\pm 30^\circ$	$\pm 40^\circ$
Max 1-dB gain BW (%)	4.3	10	25.4	28
$\Delta G$ (dB)	0.75	1.95	1.1	0.8
SLL (dB) at $30^\circ$	-12	-15	-18.4	-15.6

## Conclusions

In this paper, a dielectric UC is used to design a reflectarray with favorable beam-steering capabilities and enhanced bandwidth. After having checked the performance of the UC, a bifocal reflectarray has been designed, manufactured with a 3D printer and experimentally characterized. The results confirm the RA's good scanning capabilities, characterized by gain losses of the order of 0.8 dB over a  $\pm 40^\circ$  scan range, while the measured 1-dB bandwidth is attested to vary from 13% up to 28% over the entire scanning region. These results demonstrate the capability of 3D-printing technology for producing high-performance, cost-effective reflectarray antennas with wideband behavior and excellent beam-steering capabilities. Moreover, the proposed bifocal approach applied to a dielectric-only RA highlights the potential for a wide range of practical applications, from radars to wireless networking. A further improvement of this feature can be obtained adopting a proper optimization technique, like that used in [42], for the design of a beam-scanning reflectarray.

## References

- Huang J and Encinar JA (2008) *Reflectarray Antennas*. Hoboken, NJ: Wiley-IEEE press.
- Nayeri P, Yang F and Esherbani AZ (2018) *Reflectarray Antennas: Theory, Designs and Applications*. Hoboken, NJ, USA: Wiley.
- Encinar JA (2001) Design of two-layer printed reflectarray using patches of variable size. *IEEE Transactions on Antennas and Propagation* **49**(10), 1403–1410.
- Encinar JA and Zornoza JA (2003) Broadband design of three-layer printed reflectarrays. *IEEE Transactions on Antennas and Propagation* **51**(7), 1662–1664.
- Chaharmir MR, Shaker J and Legay H (2009) Broadband design of a single layer large reflectarray using multi cross loop elements. *IEEE Transactions on Antennas and Propagation* **57**(10), 3363–3366.
- Yoon JH, Yoon YJ, Lee W-S and So J-H (2015) Broadband microstrip reflectarray with five parallel dipole elements. *IEEE Antennas and Wireless Propagation Letters* **14**, 1109–1112.
- Wang Q, Shao ZH, Cheng YJ and Li PK (2015) Broadband low-cost reflectarray using modified double-square loop loaded by spiral stubs. *IEEE Transactions on Antennas and Propagation* **63**(9), 4224–4229.
- Li X, Li X, Luo Y, Wei G and Yi X (2021) A novel single layer wide-band reflectarray design using two degrees of freedom elements. *IEEE Transactions on Antennas and Propagation* **69**(8), 5095–5099.
- Kundu D, Bhattacharya D and Ruchi R (2022) A single-layer broadband reflectarray in K-band using cross-loop slotted patch elements. *IEEE Access* **10**, 13490–13495.
- Zhang S (2017) Three-dimensional printed millimetre wave dielectric resonator reflectarray. *IET Microwaves, Antennas & Propagation* **11**(14), 2005–2009.
- Wu MD, Li B, Zhou Y, Guo DL, Liu Y, Wei F and Lv X (2018) Design and measurement of a 220 GHz wideband 3-D printed dielectric reflectarray. *IEEE Antennas and Wireless Propagation Letters* **17**(11), 2094–2098.
- Zhao X, Wei F, Li B and Shi X (2018) Design of circularly polarized dielectric resonator reflectarray antenna. *The Asia-Pacific Microwave Conference (APMC)*. Kyoto, Japan: IEEE. 1552–1554.
- Mei B, Zhang S and Pedersen GF (2020) A wideband 3-D printed reflectarray antenna with mechanically Reconfigurable Polarization. *IEEE Antennas and Wireless Propagation Letters* **19**(10), 1798–1802.
- Li B, Mei CY, Zhou Y and Lv X (2020) A 3-D-printed wideband circularly polarized dielectric reflectarray of cross-shaped element. *IEEE Antennas and Wireless Propagation Letters* **19**(10), 1734–1738.
- Cui Y, Nauroze SA, Bahr R and Tentzeris EM (2020) 3d printed one-shot deployable flexible “Kirigami” dielectric reflectarray antenna for mm-wave applications. *IEEE MTT-S International Microwave Symposium Digest*. Los Angeles, CA: IEEE. 1164–1167.
- Cheng Q, Hao Y, McGhee J, Whittow WG, Cheng Q, Vardaxoglou JC, Mittra R and Zhang S (2022) Dual circularly polarized 3-D printed broadband dielectric reflectarray with a linearly polarized feed. *IEEE Transactions on Antennas and Propagation* **70**(7), 5393–5403.
- Yu H, Li P, Su J, Li Z, Xu S and Yang F (2022) Reconfigurable bidirectional beam-steering aperture with transmitarray, reflectarray, and transmit-reflect-array modes switching. *IEEE Transactions on Antennas and Propagation*, **70**(1), 581–595.
- Xiang BJ, Dai X and Luk K-M (2022) A wideband low-cost reconfigurable reflectarray antenna with 1-bit resolution. *IEEE Transactions on Antennas and Propagation* **70**(9), 7439–7447.
- Lee S-G, Nam Y-H, Kim Y, Kim J and Lee J-H (2022) A wide-angle and high-efficiency reconfigurable reflectarray antenna based on a miniaturized radiating element. *IEEE Access* **10**, 103223–103229.

20. Zhang N, Chen K, Zhao J, Hu Q, K Tang, Zhao J, Jiang T and Feng Y (2022) A dual-polarized reconfigurable reflectarray antenna based on dual-channel programmable metasurface. *IEEE Transactions on Antennas and Propagation* **70**(9), 7403–7412.
21. Xi B, Xiao Y, Zhu K, Liu Y, Sun H and Chen Z (2022) 1-Bit wideband reconfigurable reflectarray design in Ku-band. *IEEE Access* **10**, 4340–4348.
22. Wu F, Lu R, Wang J, Jiang ZH, Hong W and Luk K-M (2022) Circularly polarized one-bit reconfigurable ME-dipole reflectarray at X-band. *IEEE Antennas and Wireless Propagation Letters* **21**(3), 496–500.
23. Li H, Qi X, Zhou T, Xu Z and Denidni TA (2022) Wideband reconfigurable reflectarray based on reflector-backed second-order bandpass frequency selective surface. *IEEE Transactions on Antennas and Propagation*, **70**(12), 12334–12339.
24. Zhou S-G, Zhao G, Xu H, Luo C-W, Sun J-Q, Chen G-T and Jiao Y-C (2022) A wideband 1-bit reconfigurable reflectarray antenna at Ku-band. *IEEE Antennas and Wireless Propagation Letters* **21**(3), 566–570.
25. Baracco J-M, Ratajczak P, Brachet P, Fargeas J-M and Toso G (2022) Ka-band reconfigurable reflectarrays using varactor technology for space applications: A proposed design. *The IEEE Antennas and Propagation Magazine* **64**(1), 27–38.
26. Nam I-J, Lee S and Kim D (2022) Miniaturized beam reconfigurable reflectarray antenna with wide 3-D beam coverage. *IEEE Transactions on Antennas and Propagation* **70**(4), 2613–2622.
27. Liu X, Schmitt L, Sievert B, Lipka J, Geng C, Kolpatzck K, Erni D, Rennings A, Balzer JC, Hoffmann M and Czylwik A (2022) Terahertz beam steering using a MEMS-based reflectarray configured by a genetic algorithm. *IEEE Access* **10**, 84458–84472.
28. Kim H, Kim J and Oh J (2022) A novel systematic design of high-aperture-efficiency 2D beam-scanning liquid-crystal embedded reflectarray antenna for 6G FR3 and radar applications. *IEEE Transactions on Antennas and Propagation* **70**(11), 11194–11198.
29. Li X, Sato H, Shibata Y, Ishinabe T, Fujikake H and Chen Q (2022) Development of beam steerable reflectarray with liquid crystal for both E-plane and H-plane. *IEEE Access* **10**, 26177–26185.
30. Zhang W, Li Y and Zhang Z (2022) A reconfigurable reflectarray antenna with an 8  $\mu\text{m}$ -thick layer of liquid crystal. *IEEE Transactions on Antennas and Propagation* **70**(4), 2770–2778.
31. Carrasco E, Gomez-Cruz J, Serrano-Berruero M, Saavedra CE and Escobedo C (2022) Design of microfluidic reflectarray elements for multi-reconfiguration using liquid metal. *IEEE Open Journal of Antennas and Propagation* **3**, 425–434.
32. Zhang H, Wu W, Cheng Q, Chen Q, Yu Y-H and Fang D-G (2022) Reconfigurable reflectarray antenna based on hyperuniform disordered distribution. *IEEE Transactions on Antennas and Propagation* **70**(9), 7513–7523.
33. Rubio AJ, Kaddour A-S and Georgakopoulos SV (2022) A mechanically rollable reflectarray with beam-scanning capabilities. *IEEE Open Journal of Antennas and Propagation* **3**, 1180–1190.
34. Nayeri P, Yang F and Elsherbeni AZ (2015) Beam-scanning reflectarray antennas: A technical overview and state of the art. *IEEE Transactions on Antennas and Propagation* **57**(4), 32–47.
35. Wu G-B, Qu S-W and Yang S (2018) Wide-angle beam-scanning reflectarray with mechanical steering. *IEEE Transactions on Antennas and Propagation* **66**(1), 172–181.
36. Mei P, Zhang S and Pedersen GF (2020) A low-cost, high-efficiency and full-metal reflectarray antenna with mechanically 2-D beam-steerable capabilities for 5G applications. *IEEE Transactions on Antennas and Propagation* **68**(10), 6997–7006.
37. Nayeri P, Yang F and Elsherbeni AZ (2013) Bifocal design and aperture phase optimizations of reflectarray antennas for wide-angle beam scanning performance. *IEEE Transactions on Antennas and Propagation* **61**(9), 4588–4597.
38. Cui Y, Bahr R, Nauroze SA, Cheng T, Almoneef TS and Tentzeris MM (2022) 3D printed ‘Kirigami’-inspired deployable bi-focal beam-scanning dielectric reflectarray antenna for mm-wave applications. *IEEE Transactions on Antennas and Propagation* **70**(9), 7683–7690.
39. Pirinoli P, Lohrey T, Orefice M, Beccaria M and Dassano G (2021) Multifocal approach for reflectarray antenna for DTH applications. *15th European Conference on Antennas and Propagation (EuCAP)*. Dusseldorf, Germany: IEEE. 1–4.
40. Pirinoli P, Lohrey T, Orefice M, Beccaria M and Dassano G (2019) Reflectarray with mechanically steerable beam for DTH application, *49th European Microwave Conference (EuMC)*. Paris, France: IEEE. 141–144.
41. Wu G-B, Qu S-W, Yang S and Chan CH (2020) Low-cost 1-D beam-steering reflectarray with  $\pm 70^\circ$  scan coverage. *IEEE Transactions on Antennas and Propagation* **68**(6), 5009–5014.
42. Niccolai A, Beccaria M, Zich RE, Massaccesi A and Pirinoli P (2020) Social network optimization based procedure for beam-scanning reflectarray antenna design. *IEEE Open Journal of Antennas and Propagation* **1**, 500–512.
43. Massaccesi A, Beccaria M and Pirinoli P (2019) 3D-printable perforated dielectric reflectarray in Ka-band, *2019 IEEE International Symposium on Antennas and Propagation*. Atlanta, Georgia, USA: IEEE. 295–296.
44. Massaccesi A, Beccaria M and Pirinoli P (2022) Beam steering mm-waves dielectric-only reflectarray, *Maternal Mirror Syndrome (MMS) Pizzo* Calabro, Italy: IEEE, 1–4.
45. Massaccesi A, Pirinoli P, Bertana V, Scordo G, Marasso SL, Cocuzza M and Dasasano G (2018) 3D-Printable dielectric transmitarray with enhanced bandwidth at millimeter-waves. *IEEE Access* **6**, 46407–46418.
46. Massaccesi A, Dassano G and Pirinoli P. (2019) Beam scanning capabilities of a 3D-printed perforated dielectric transmitarray. *Electronics* **8**(4), 379.
47. Beccaria M, Addamo G, Orefice M, Peverini O, Manfredi D, Calignano F, Virone G and Pirinoli P (2021) Enhanced efficiency and reduced side lobe level convex conformal reflectarray. *Applied Sciences* **11**(21), 9893.



**Andrea Massaccesi** was born in Osimo, Italy, in 1987. He received the B.S. degree in electronic engineering from the Università Politecnica delle Marche, Ancona, Italy, in 2012, the M.S. degree in electronic engineering and the Ph.D. degree (cum laude) in electrical, electronic and communication engineering from the Politecnico di Torino, Turin, Italy, in 2015 and 2019, respectively. From November 2017 to May 2018, he was a visiting Ph.D. student with Loughborough University, Loughborough, UK, within the Symeta research program. Since January 2020, he has been a research fellow with the Department of Electronics and Telecommunications, Politecnico di Torino, Turin, Italy. His research activities include the study of underwater electromagnetic propagation and the design of proper antennas for underwater environments, the design and manufacturing of transmitarray and reflectarray antennas exploiting 3D-printing techniques, and the development of efficient global optimization techniques suitable for electromagnetic problems.



**Michele Beccaria** was born in Enna, Italy, on July 24, 1991. He received the B.Sc. the M.Sc. degree, and the Ph.D. degree (cum laude) in applied electromagnetics from the Politecnico di Torino in 2013, 2015, and 2019, respectively. He has been a research fellow with the Department of Electronics and Telecommunications, Politecnico di Torino, Turin, since January 2019 and has been an Assistant Professor since 2023. In 2017 and 2018, he was a visiting Ph.D. student with Tsinghua University, Beijing, China, under the supervision of Prof. Fan Yang. His research interests include reflectarray antennas, transmitarray antennas, smart electromagnetic surfaces, and the application of new optimization algorithms for complex antenna design. He was also recognized as the winner of two grants for attending the Ph.D. courses of ESoA in 2016 and in 2018 as one of the Best Ph.D. Students at Politecnico di Torino with the Ph.D. Quality Award. He was included in the Technical Committee of Conference of International Relevance (ICCE 2018, 2020) and serves many journals of the IET group as a reviewer. In 2020, he received the



2019 IEEE AP/ED/MTT North Italy Chapter Thesis Awards with the Best Ph.D. Thesis Antennas and Propagation Society for the thesis “Design of Innovative Reflectarray and Transmitarray Antennas.”



**Valentina Bertana** received her B.Sc. and M.Sc. Degree in biomedical engineering at Politecnico di Torino in 2013 and 2015, respectively. In February 2020, she received her Ph.D. degree at Politecnico di Torino in electrical, electronic and communication engineering. Her research activities are mainly focused on AM, smart materials, printable electronics, and microfluidics.



**Simone Luigi Marasso** received his Master degree in biomedical engineer and Ph.D. degree in electronic devices from Politecnico di Torino, Turin, Italy, in 2005 and 2010, respectively. From 2005 to 2011, he had a fellowship with Politecnico di Torino, Turin, Italy, and he worked at Chilab, materials and microsystem laboratory at Chivasso, Italy. Since 2014, he is a CNR researcher, IMEM, @Politecnico di Torino DISAT department. His research activities

focus on design and fabrication of MEMS, Lab on Chip and microfluidic devices as demonstrated by his scientific publications in these fields.



**Matteo Cocuzza** obtained the degree in electronic engineering at the Polytechnic of Turin in 1997 and the PhD in electronic devices in 2003. He is currently Associate Professor at the Department of Applied Science and Technology of the Polytechnic of Turin and associate researcher of IMEM-CNR. In 1998, he was one of the founders of the Chilab-Materials and Microsystems Laboratory and recently the co-founder of the new technological facility PiQuET –

Piedmont Quantum Enabling Technologies. He is currently lecturer of master's degree courses in the field of micro- and nanotechnologies, microsensors,

MEMS, also in the context of the international master in nanotechnology for ICT (joint master between Politecnico di Torino, INPG Grenoble and EPFL Lausanne). His research activity is focused on the development of MEMS and microsensors for industrial applications, on the development of microfluidics and lab-on-a-chip for biomedical applications, and more recently, on the development and application of 3D printing polymeric technologies.

**Gianluca Dassano** received the Laurea degree in electronic engineering from the Politecnico di Torino, Italy, in 1999. Since 1999, he has been with the Department of Electronics and Telecommunications, Politecnico di Torino, as a Technician with the Electromagnetic Group, with particular interest in antenna application. At present, his main activities concern antenna prototyping and characterization inside the Laboratory of Antennas and EMC.



**Paola Pirinoli** received the M.S. (Laurea) and Ph.D. (Dottorato di Ricerca) degrees in electronic engineering from the Politecnico di Torino, Italy, in 1989 and 1993, respectively. From 1994 to 2003, she was an Assistant Professor (Ricercatore) of electromagnetic fields with the Department of Electronics and Telecommunications, Politecnico di Torino, where she was an Associate Professor from 2003 to 2018 and has been a Full Professor since 2018. From 1996

to 1997, she was a Visiting Research Fellow with the University of Nice, Sophia Antipolis, France. In 2014, 2015, and 2017, she was a Visiting Research Fellow with Tsinghua University, Beijing, China. She has coauthored around 250 journal articles and conference papers. Her main research activities include the development of analytically based numerical techniques, essentially devoted to the fast and accurate analysis of printed structures on planar or curved substrates, the modeling of nonconventional substrates, as chiral and anisotropic ones, the development of innovative and efficient global optimization techniques, and the design of innovative reflectarray and transmitarray antennas. In 1998, she received the URSI Young Scientist Award and the Barzilai Prize for the Best Paper at the National Italian Congress of Electromagnetic (XII RiNEM). In 2000, she was the recipient of the Prize for the Best Oral Paper on Antennas at the Millennium Conference on Antennas and Propagation. She serves as a reviewer for several international journals and conferences. She is a member of the TPC and the organizing committee of several international conferences.